Journal of Marine Science and Technology, Vol. 24, No. 6, pp. 1217-1225 (2016)
DOI: 10.6119/JMST-016-1026-10

RECONSTRUCTION AND ANALYSIS OF SURFACE VELOCITY FROM DRIFTERS IN THE KUROSHIO REGION EAST OF TAIWAN

Kai-Ho Cheng, Chen-Chih Lin, Po-Chun Hsu, and Shih-Jen Huang

Key words: DINEOF, drifter, Kuroshio, Taiwan.

ABSTRACT

In this study, sea surface velocities derived from drifters were gridded to 0.25° latitude by 0.25° longitude for analysis of the Kuroshio region east of Taiwan. The data for each grid that were originally missing were obtained using the Data Interpolating Empirical Orthogonal Functions (DINEOF) method, which can precisely reconstruct missing data. Compared with the original data, the error of the reconstructed Kuroshio velocity is 0.18 ± 0.03 m/s. By analyzing the reconstructed data, we defined the Kuroshio axis at its maximum surface velocity in the zonal direction of 0.25° latitude along the east coast of Taiwan. The results indicate that the Kuroshio flows faster in summer than it does in winter because of monsoon effects. With the exception of 2010, the Kuroshio was observed to commonly move inshore in winter and offshore in summer in the time span of this study.

I. INTRODUCTION

Taiwan is located in the northwest Pacific Ocean. The continental slope east of Taiwan is very steep and the waters are very deep. The Kuroshio is a western boundary current in the north Pacific Ocean. It origins from the North Equatorial Current. The Kuroshio brings warm water from the equator to flow northward along the east coast of Taiwan and the shelf edge of the East China Sea toward Japan. Taiwan has a subtropical climate, and because of its location it is subject to the influence of the East Asia monsoon. The northeasterly monsoon prevails between October and April, and the southwesterly monsoon prevails between May and September.

Because the Kuroshio transports heat and water from the tropical latitudes to the middle latitudes, variations in the Kuroshio's axis and velocity may affect the local climate. These variations have been investigated intensively by numerical models (e.g., Hsin et al., 2008; Kuo and Chern, 2011), in-situ measurements from cruises (e.g., Jan et al., 2015), satellite observations (e.g., Liu and Gan, 2012), and high-frequency radar data (e.g., Takahashi et al., 2006; Morimoto et al., 2009). Currently, global drifters are available for the study of ocean currents. This mode of measurement provides another opportunity to study Kuroshio variations. However, drifter observations are a type of Lagrange observation; they change with time and location. To conduct a synoptic observation of sea surface velocity derived from drifters, the velocity within the study area from 21°N to 25°N and 120.8°E to 123°E (Fig. 1) was gridded to 0.25° latitude by 0.25° longitude for a month. The Data Interpolating Empirical Orthogonal Functions (DINEOF) method was subsequently applied to reconstruct the missing data on the grids. The DINEOF method is an application of empirical orthogonal functions (EOFs) for filling incomplete datasets that was proposed by Beckers and Rixen (2003), modified by Alvera-Azcarate et al. (2005), and finally rendered complete by Beckers et al. (2006) and Alvera-Azcarate et al. (2007). After all gridded sea surface velocity

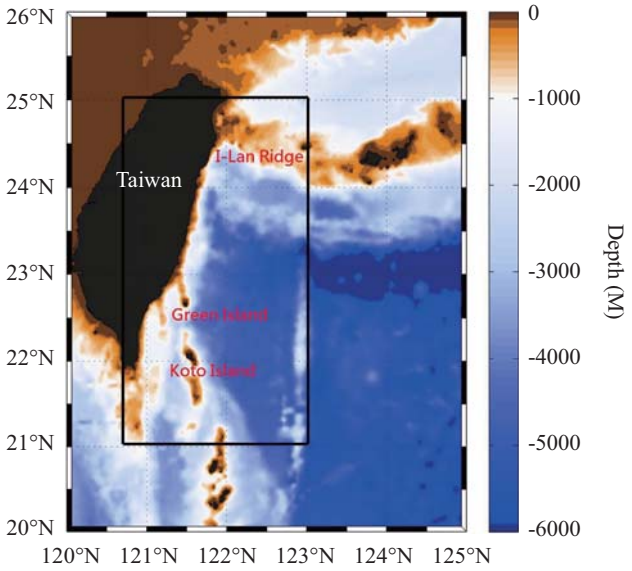

Fig. 1. Bathymetric chart around Taiwan. The rectangle indicates the study area.

Paper submitted 05/27/16; revised 06/16/16; accepted 11/28/16. Author for correspondence: Chen-Chih Lin (mikania.lin@gmail.com).
Department of Marine Environmental Informatics, National Taiwan Ocean University, Keelung, Taiwan, R.O.C.

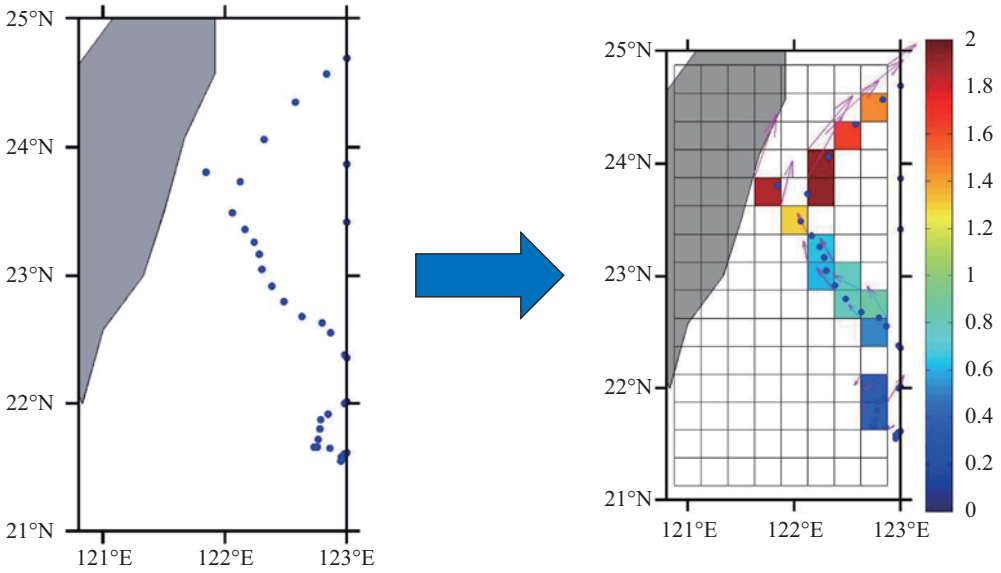

Fig. 2. Drifter track (left) and gridded velocity (right). The color bar unit is m/s.

data were available, the Kuroshio axis could be determined according to the definition proposed by Ambe et al. (2004).

II. DATA AND METHODOLOGY

The drifter data employed in this study were obtained from Fisheries and Oceans Canada (http://www.dfo-mpo.gc.ca/index-eng.htm). The Responsible National Oceanographic Data Centre of Oceanography and Scientific Data has managed a continually updated archive of data collected from drifting buoys in various parts of the world since 1978. Data can be requested based on buoy, area, date, or program, with parameters including position, air temperature, water temperature, air pressure, wind speed, and wind direction. In this study, we employed Surface Velocity Program data that were collected and processed by the Atlantic Oceanographic and Meteorological Laboratory under the Global Drifter Program (formerly the World Ocean Circulation Experiment Surface Velocity Program). The data were available from 1979 to 2011.

This study employed data spanning the period 2003-2011. We divided each year into two parts: summer (April-September) and winter (October-March). Drifters automatically send the signal of their latitude and longitude back every 6 hours through satellite positioning. The velocity of the drifters is then calculated through the following steps: First, the distance from position to position in spherical coordinates is calculated with the Haversine method as follows:

$$d = 2R \times \sin^{-1}\left(\sqrt{\sin^2\left(\frac{\phi_2 - \phi_1}{2}\right) + \cos\phi_1 \cos\phi_2 \sin^2\left(\frac{\lambda_2 - \lambda_1}{2}\right)}\right), \quad (1)$$

where d is the distance, R is the earth radius (6378.137 km), Φ is the latitude, and λ is the longitude. Second, the velocity is derived by dividing the distance by the time. Third, the calculated velocity is then plotted in a 0.25° by 0.25° grid to obtain the gridded velocity field (Fig. 2).

After conducting the aforementioned steps to obtain the semiannual gridded velocity data, some data were still missing (Fig. 3). To reconstruct and fill in the missing gridded velocity data, we applied the DINEOF method. The original data **X** constitute a matrix of $m \times n$ ($m > n$), where m is the spatial dimension of the drift data, and n is the temporal dimension of the drift data, expressed as follows:

$$\mathbf{X} = \mathbf{UDV}^{\mathrm{T}} \quad (2)$$

where **U** is a matrix of $m \times r$ that represents the decomposition of spatial EOFs, **V** is a matrix of $r \times n$ that represents the decomposition of temporal EOFs, and **D** is the diagonal element of the matrix containing singular values. Subsequently, the reconstructed function can be applied to obtain reconstructed values as follows:

$$\mathbf{X} = \mathbf{UDV}^{\mathrm{T}} = \sum_{k=1}^{q} \rho_k u_k v_K^{\mathrm{T}}. \quad (3)$$

where ρ is the singular value, and u and v are the eigenvectors. Rank q ≤ min (m, n). Because the EOFs require a complete matrix without missing data, DINEOF is necessary to process the missing point. Let **I** be the ensemble of discrete points where data are incomplete. Each missing data point (i, j) belongs to I. $\mathbf{X_0}$ is the original dataset from which data are missing, and $\mathbf{X}_a$ is the reconstructed result. $\mathbf{X}^e$ is the reconstruction of the corresponding matrix by the first N EOFs for any of these matrices.

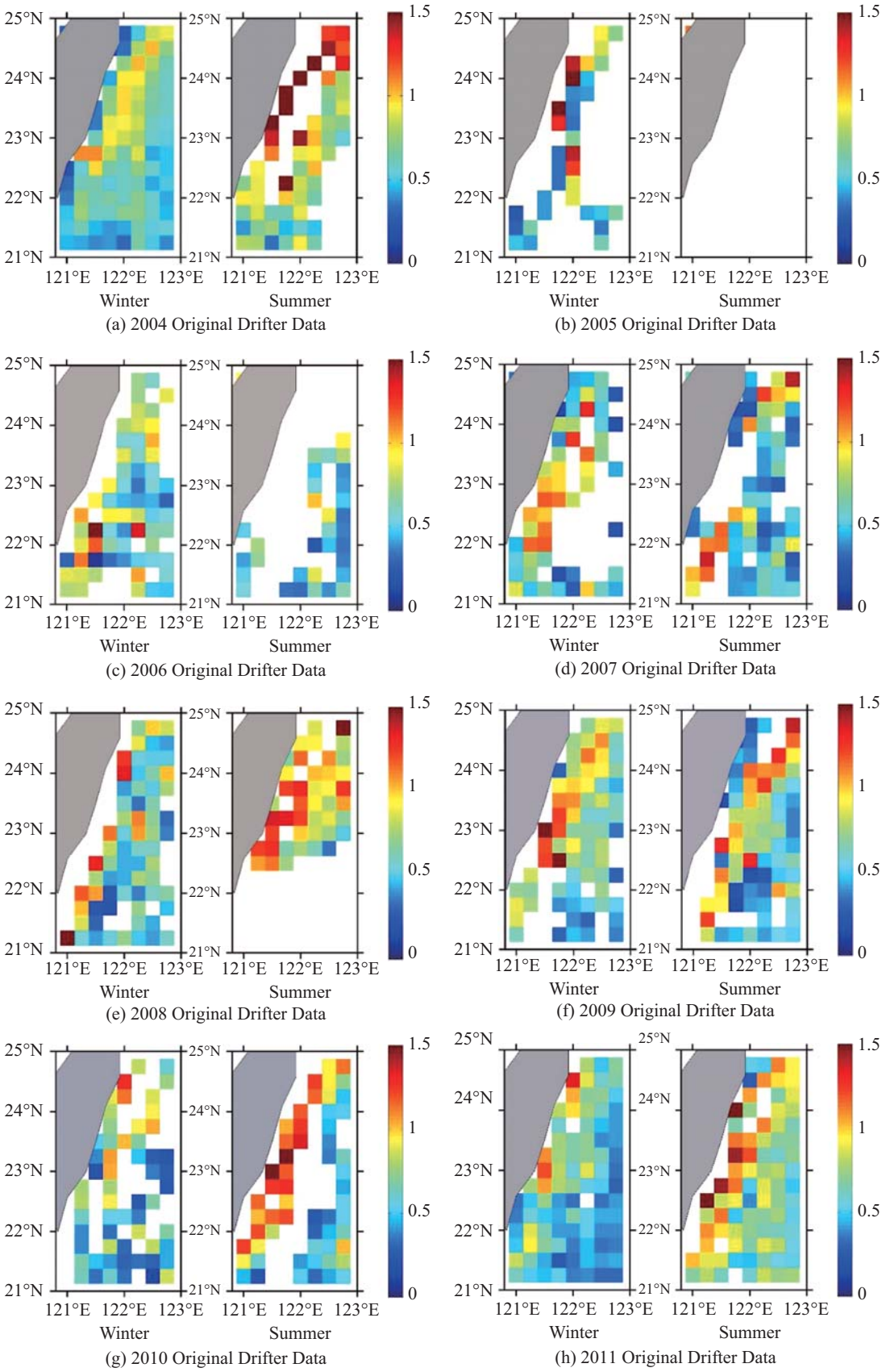

Fig. 3. Original gridded drifter velocities from 2004 to 2011 in winter (left) and summer (right). Blank spaces denote that no drifter is present. The color bar unit is m/s.

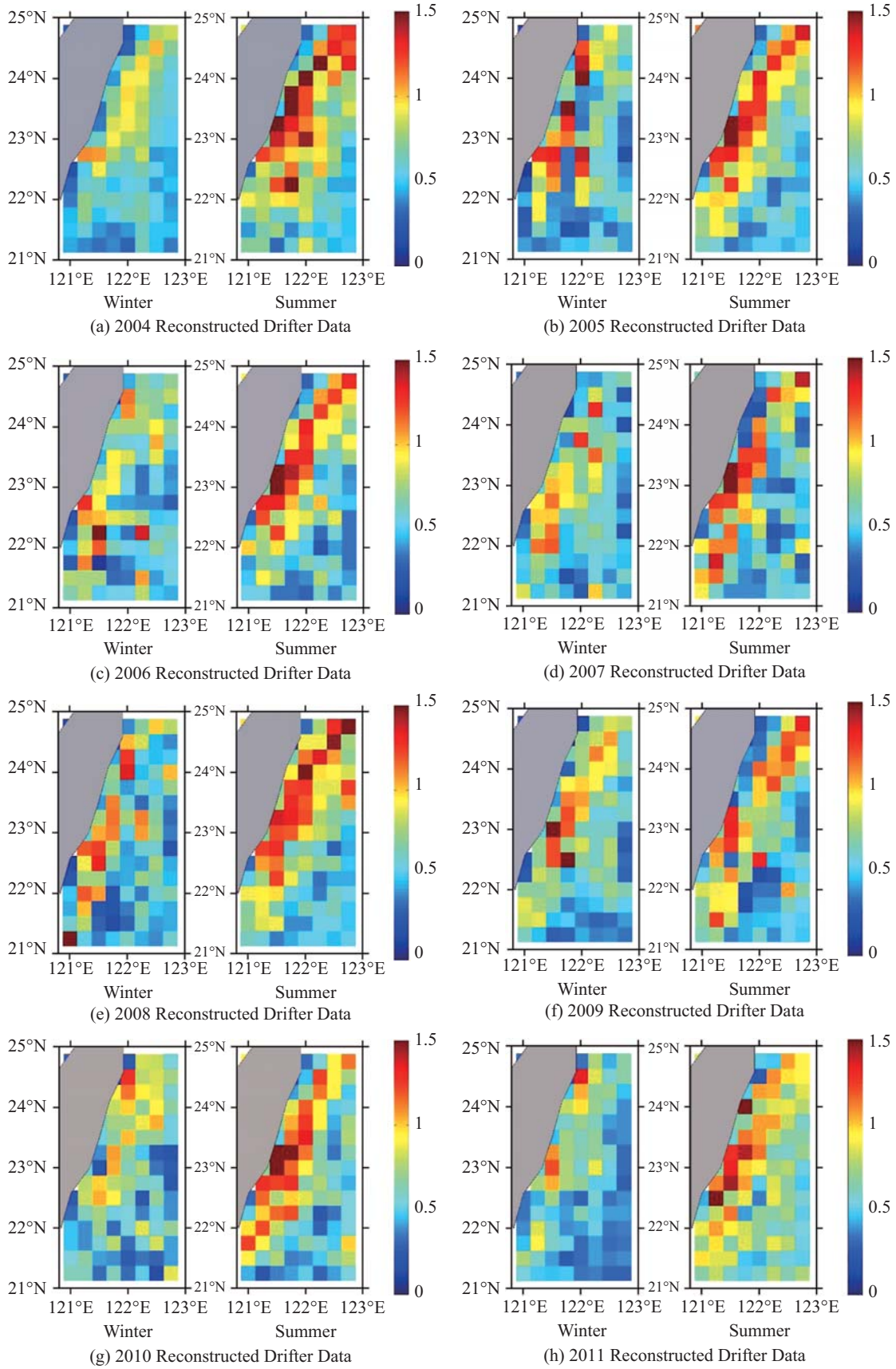

Fig. 4. Reconstructed velocities from 2004 to 2011 in winter (left) and summer (right). The blank grids in Fig. 3 are filled in by the reconstructed data.

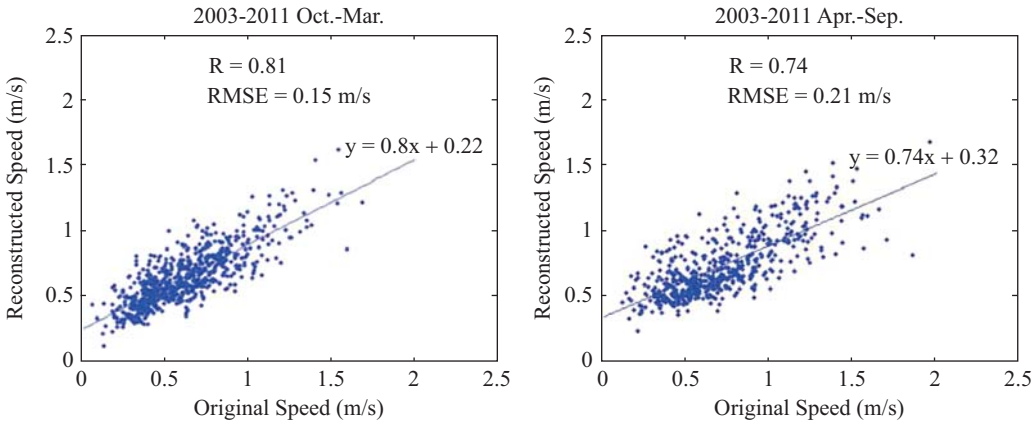

Fig. 5. Scatter plot of original data with reconstructed data for winter (left) and summer (right).

Table 1. Missing ratios of data points and correlation coefficients between original data and reconstructed data for the period 2004-2011.

Year		2004	2005	2006	2007	2008	2009	2010	2011
Missing ratio (%)	Summer	45.6	99.2	64.0	32.0	60.0	24.0	42.4	16.0
	winter	2.4	70.4	36.8	43.2	35.2	23.4	40.8	8.8
Corr. coefficient	Summer	0.69	*	0.63	0.7	0.73	0.73	0.86	0.71
	winter	0.76	0.95	0.73	0.84	0.68	0.84	0.85	0.79

* Only one item of data is available for 2005.

First, we apply a value of 0 for all missing data points [$(i, j) \in \mathbf{I}$] within the matrix. Let $\mathbf{X_0}$ be the matrix that has observed points subtracted by the average values of temporal dimensions. Then, the singular value decomposition (SVD) method is applied to $\mathbf{X}$ to obtain the decomposition of spatial and temporal EOFs. Missing data points [$(i, j) \in \mathbf{I}$] are obtained through an EOF series as follows:

$$(\mathbf{X}_a)_{ij} = (\mathbf{U}_N \mathbf{D}_N \mathbf{V}_N^{\mathrm{T}})_{ij} = (\mathbf{X}_0^e)_{ij} = \sum_{k=1}^{N} \rho_k (u_k)_i (v_k^{\mathrm{T}})_j, \quad (i, j) \in \mathbf{I} \tag{4}$$

The preceding function applies only in the first N spatial EOFs. Therefore, $\mathbf{X}_a$ is expressed as

$$\mathbf{X}_a = \mathbf{X}_0 + \delta\mathbf{X} \tag{5}$$

where the matrix $\delta\mathbf{X}$ is always zero, except at the missing data points. After the missing data points are replaced by their new values, the same procedure is repeated. The following set of operations is performed until convergence occurs:

$$\mathbf{U}\mathbf{D}\mathbf{V}^{\mathrm{T}} = \mathbf{X}_a \tag{6}$$

$$(\mathbf{X}_a)_{ij} = (\mathbf{U}_N \mathbf{D}_N \mathbf{V}_N^{\mathrm{T}})_{ij} = (\mathbf{X}_a^e)_{ij} = \sum_{k=1}^{N} \rho_k (u_k)_i (v_k^{\mathrm{T}})_j, \quad (i, j) \in \mathbf{I} \tag{7}$$

The EOFs converge when two consecutive SVD results are less than 10^{-8}.

The method for identifying the Kuroshio axis is based on the algorithm developed by Ambe et al. (2004). We set the grid with maximum velocity as an initial point in three adjacent grids (21°N, 120.875°E-121.375°E). Subsequently, we determined the location of the axis at the following latitude by selecting the maximum velocity in three adjacent grids above the previous grid. We then matched the maximum points in each degree of latitude to form the Kuroshio axis.

III. RESULTS

1. Reconstructed Velocity

Fig. 3 illustrates the gridded surface velocities of the drifters in the Kuroshio region east of Taiwan. A blank area denotes that no drifter is present. These blank areas can be reconstructed with the DINEOF method. Fig. 4 presents the reconstructed results, showing that the blank areas have been filled in. The DINEOF method, which can preserve the physical characteristics of the original data and estimate values for large amounts of missing data precisely, is different from the interpolation method.

2. Error Analysis

Because the DINEOF method can reconstruct data in each grid, we were able to compare the reconstructed values with the original values to evaluate errors. The correlation coefficient and root mean squared error (RMSE) were calculated to determine the accuracy of the DINEOF method. The scatter diagrams of original data with reconstructed data for summer and winter are presented in Fig. 5. The correlation coefficients were 0.74 and 0.81, and the RMSEs were 0.21 m/s and 0.15 m/s for summer and winter, respectively. The confidence of each correlation coefficient was tested. All *p*-values were lower than 0.01. Table 1 illustrates the ratio of missing data and correlation coefficients between the original data and the reconstructed data for the period 2004-2011. The lowest proportion of missing data was 2.4% in winter 2004; its correlation coefficient was 0.76. In

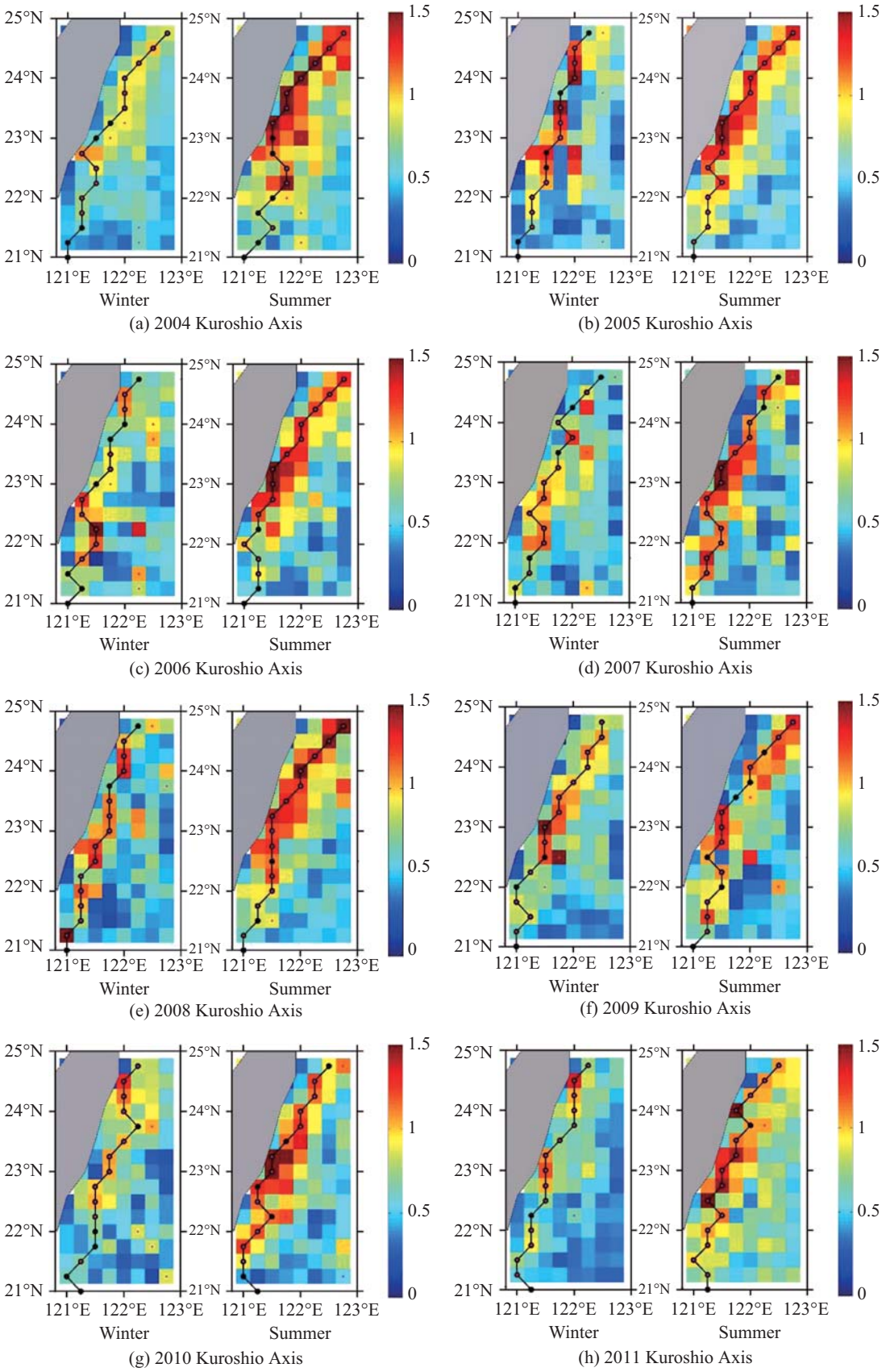

Fig. 6. Kuroshio axis in winter (left) and summer (right) for the period 2004-2011. Black points indicate maximum velocity in zonal directions with 0.25° latitude. The black line represents the Kuroshio axis.

Table 2. Correlation coefficients and RMSEs at various masking ratios.

Missing data ratio (%)	10	20	30	40	50
Corr. coefficient	0.58	0.77	0.78	0.53	0.64
RMSE (m/s)	0.29	0.22	0.19	0.28	0.24

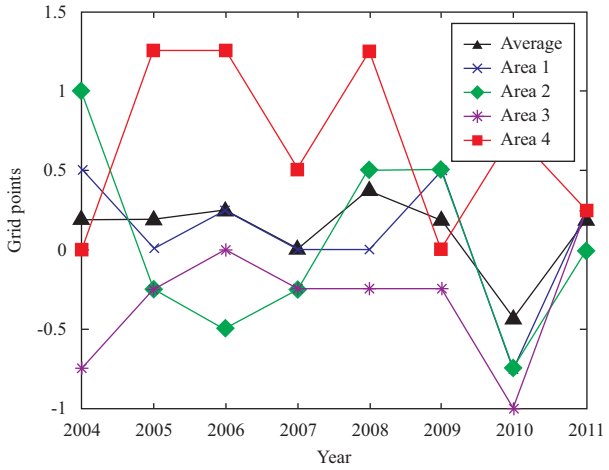

Fig. 7. Values at the y-axis indicate variations in the location of the axis between summer and winter. Black line: mean position of the Kuroshio axis; blue line: Area 1 (21°N-22°N); green line, Area 2 (22°N-23°N); pink line: Area 3 (23°N-24°N); red line: Area 4 (24°N-25°N).

winter 2005, the proportion of missing data was 70.4%; its correlation coefficient was 0.95.

To estimate the distortion of raw data through the DINEOF method, we randomly masked 10%, 20%, 30%, 40%, and 50% of the original data to use them as missing data, and subsequently reconstructed the missing data. Correlation coefficients and RMSEs were calculated between the reconstructed values and their original values. Table 2 presents the correlation coefficients and RMSEs of various masking ratios. The results indicate that no significant relationship between the proportion of missing data and the reconstruction error existed.

3. Kuroshio Axis

The Kuroshio axis is represented by the black solid line in Fig. 6. Kuroshio flow was observed to be faster and narrower with a more apparent axis in summer than in winter. To further investigate Kuroshio variations at different latitudes, we separated the study area into four smaller areas with the following latitudes: Area 1 (21°N-22°N), Area 2 (22°N-23°N), Area 3 (23°N-24°N), and Area 4 (24°N-25°N). Fig. 7 illustrates the migration of the axis location in all four areas. The values at the y-axis indicate variations in the location of the axis between summer and winter. A positive value implies that the Kuroshio axis is inshore in winter and offshore in summer, and a negative value implies that it is offshore in winter and inshore in summer. The average Kuroshio axis evidently moved offshore from Taiwan

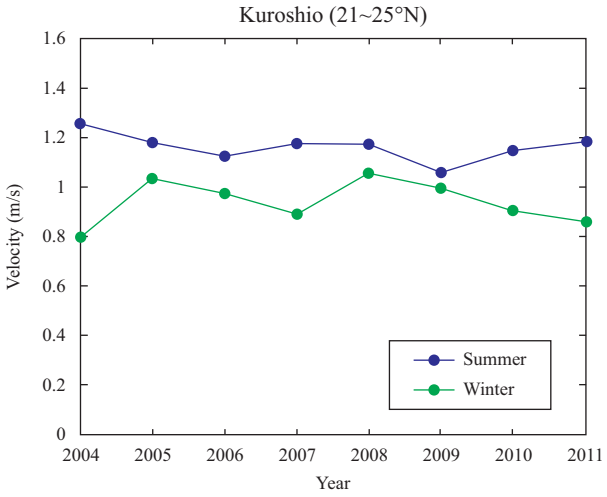

Fig. 8. Kuroshio velocities east of Taiwan in summer and winter.

during summer in each year of this study, except for 2010. However, most of the values in Area 3 are negative, suggesting the migration trend of the Kuroshio axis to have been offshore in winter, yet the positive values in Area 4 imply that the migration trend of the axis was inshore in winter.

4. Kuroshio Velocity

Fig. 8 presents the mean Kuroshio velocity between 2004 and 2011. The mean velocity was 1.16 m/s in summer and 0.94 m/s in winter. For Areas 1 to 4, the average velocities in summer were 0.88 m/s, 1.17 m/s, 1.35 m/s, and 1.25 m/s, respectively. In winter, they were 0.75 m/s, 1.02 m/s, 1.00 m/s, and 0.99 m/s, respectively. These results indicate that the velocity of the Kuroshio is higher in summer than it is in winter. In addition, Fig. 9 presents a comparison among the areas. In both summer and winter, the velocities in Areas 3 and 4 were higher than those in Areas 1 and 2. Since drifters are on the sea surface, the velocity is not only influenced by geostrophic effects but also driven by the wind. In summer, the southwesterly monsoon is positioned over the Kuroshio region; therefore, the drifter velocity may be increased as a result of the wind effect. However, the northeasterly monsoon in winter may reduce the velocity of the northward Kuroshio.

IV. DISCUSSION AND CONCLUSIONS

The surface velocity of drifters in the Kuroshio region east of Taiwan was calculated and reconstructed using the DINEOF method. In addition, to render the reconstructed data more trustworthy, we selected the spatial locations of drifters at strong current areas, such as the location of the western boundary current. By analyzing the location of the Kuroshio axis, we observed that it moved offshore from Taiwan in a northeasterly direction in summer in all years of this study except for 2010. In Area 4, the Kuroshio axis was observed to deflect near the Ilan Ridge and move east near northeast Taiwan. The same situation was observed by Liang et al. (2003). By contrast, the

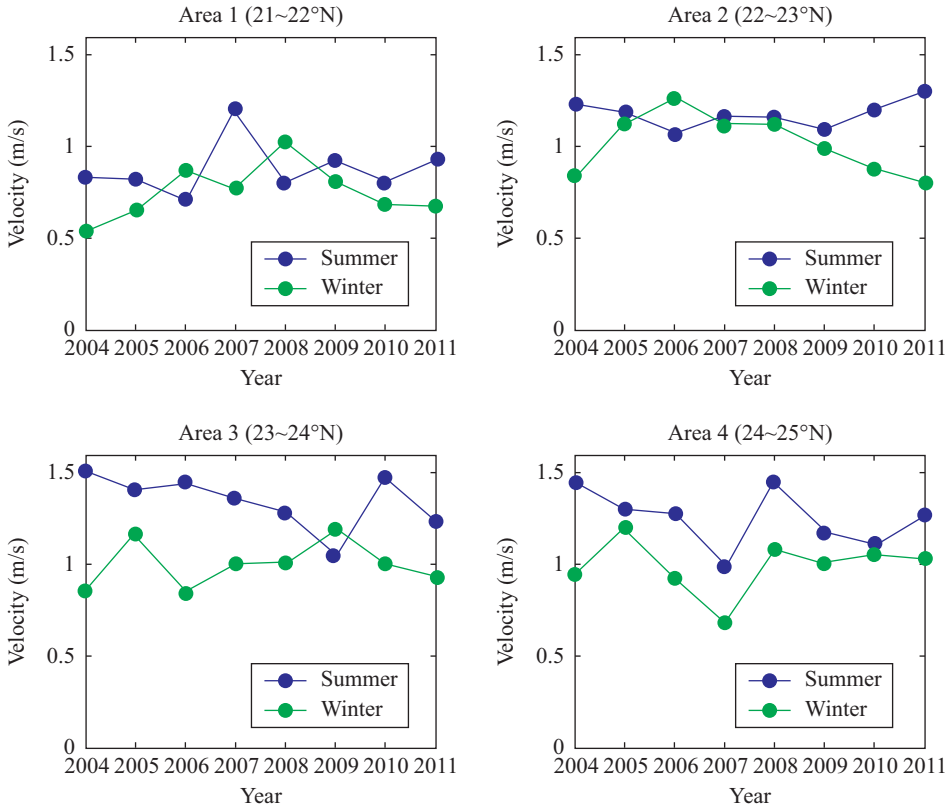

Fig. 9. Kuroshio velocities in Areas 1 to 4 in summer and winter.

results for Areas 1 and 2 were different from those of Hsin and Qiu (2013), likely because drifters flow on the sea surface, and therefore may be affected by wind and geostrophic effects. This implies that although the Kuroshio is a geostrophic current, the wind effect cannot be ignored, especially on the sea surface. The velocity analysis revealed that the Kuroshio flows faster in summer than in winter, likely because of the monsoon effects. The Kuroshio velocities in Areas 3 and 4 were higher than those in Areas 1 and 2, likely because the flow is forced by the conservation of potential vorticity, which can increase velocity with a higher latitude. The velocity in Area 3 was higher than that in Area 4 because the axis in Area 3 was closer to land, and thus, the land effect forced the Kuroshio flow to accelerate.

ACKNOWLEDGEMENTS

Drifter data used in this study was accessed from Fisheries and Oceans Canada (http://www.dfo-mpo.gc.ca/index-eng.htm). This work was supported by the Ministry of Science and Technology of Taiwan through grant MOST 103-2611-M-019-006. The traveling support for attending the conferences held in Kinmen and HongKong by National Natural Science Foundation of China under project U1405233 is also acknowledged.

REFERENCES

Alvera-Azcárate, A., A. Barth, M. Rixen and J.-M. Beckers (2005). Reconstruction of incomplete oceanographic data sets using Empirical Orthogonal Functions application to the Adriatic Sea. Ocean Modelling 9, 325-346.

Alvera-Azcárate, A., A. Barth, J.-M. Beckers and R. H. Weisberg (2007). Multivariate reconstruction of missing data in sea surface temperature, chlorophyll and wind satellite fields. Journal of Geophysical Research: Oceans 112, C03008.

Ambe, D., S. Imawaki, H. Uchida and K. Ichikawa (2004). Estimating the Kuroshio axis south of Japan using combination of satellite altimetry and drifting buoys. Journal of Oceanography 60, 375-382

Bechers, J.-M. and M. Rixen (2003). EOF calculations and data filling from incomplete oceanographic data sets. Journal of Atmospheric and Oceanic Technology 20, 1839-1856.

Beckers, J.-M., A. Barth and A. Alvera-Azcarate (2006). DINEOF reconstruction of clouded images including error maps: Application to the sea surface temperature around Corsican Island. Ocean Science 2, 183-199.

Hsin, Y.-C., B. Qiu, T.-L. Chiang and C.-R. Wu (2013). Seasonal to interannual variations in the intensity and central position of the surface Kuroshio east of Taiwan. Journal of Geophysical Research: Oceans 118, 4305-4316.

Hsin, Y.-C., C.-R. Wu and P.-T. Shaw (2008). Spatial and temporal variations of the Kuroshio east of Taiwan, 1982-2005: A numerical study. Journal of Geophysical Research: Oceans 113, C04002.

Jan, S., Y.-J. Yang, J. Wang, V. Mensah, T.-H. Kuo, M.-D. Chiou, C.-S. Chen, M.-H. Chang and H. Chien (2015). Large variability of the Kuroshio at 23.75°N east of Taiwan. Journal of Geophysical Research: Oceans 120, 1825-1840.

Kuo, Y.-C. and C.-S. Chern (2011). Numerical study on the interactions between a mesoscale eddy and a western boundary current. Journal of Oceanography 67, 263-272.

Liang, W.-D., T. Y. Tang, Y. J. Yang, M. T. Ko and W.-S. Chuang (2003). Upper-ocean currents around Taiwan. Deep-Sea Research Part II 50, 1085-1105.

Liu, Z. L. and J. P. Gan (2012). Variability of the Kuroshio in the East China Sea derived from satellite altimetry data. Deep-Sea Research Part I 59, 25-36.

Morimoto, A., S. Kojima, S. Jen and D. Takahashi (2009). Movement of the

Kuroshio axis to the northeast shelf of Taiwan during typhoon events, Estuarine. Coastal and shelf Science 82, 547-552.

Takahashi, D., X. Guo, A. Morimoto and S. Kojima (2006). Biweekly periodic variation of the Kuroshio axis northeast of Taiwan as revealed by ocean high-frequency radar. Continental Shelf Research 29, 1896-1907.